Sparse least-squares reverse time migration using seislets

Gaurav Dutta and Gerard T. Schuster, King Abdullah University of Science and Technology*

SUMMARY

We propose sparse least-squares reverse time migration (LSRTM) using seislets as a basis for the reflectivity distribution. This basis is used along with a dip-constrained preconditioner that emphasizes image updates only along prominent dips during the iterations. These dips can be estimated from the standard migration image or from the gradient using plane-wave destruction filters or structural tensors. Numerical tests on synthetic datasets demonstrate the benefits of this method for mitigation of aliasing artifacts and crosstalk noise in multisource least-squares migration.

INTRODUCTION

Wavelet transforms provide a compact basis for data decomposition which in turn is useful for formulating efficient signal processing and depth imaging algorithms. Such transforms usually exploit the directional properties of an image through the use of suitable basis functions. They provide a perfect reconstruction of the parameters after forward and inverse transforms, are efficient to compute, and use minimal redundancy. Thus, different wavelet-like transforms such as the digital wavelet transform (DWT), curvelets, or projection onto convex sets (POCS) algorithms are often used in geophysical applications like data compression, interpolation, data regularization and denoising (Foster et al., 1994; Dessing, 1997; Wapenaar et al., 2005; Abma and Kabir, 2006; Candes et al., 2006a,b; Herrmann et al., 2009).

Fomel and Liu (2010) introduced the theory of the seislet transform that is more suitable for representing seismic data. They use basis functions that are aligned along dominant seismic events or dips. In 2D or 3D, the basis functions from the seislet transform follow locally linear events obtained from the input data using local plane-wave destruction filters (Claerbout, 1992; Fomel, 2002). Through numerical tests, they demonstrated the superior compression, interpolation and denoising properties of the seislet transform over the digital wavelet transform.

The above listed properties of the seislet transform makes it an appealing tool for use in seismic imaging problems such as least-squares migration (LSM) or full waveform inversion (FWI). LSM has been shown to produce images with better balanced amplitudes, fewer artifacts and better resolution than standard migration (Lailly, 1984; Nemeth et al., 1999; Duquet et al., 2000; Plessix and Mulder, 2004; Dai and Schuster, 2009; Tang, 2009; Wong et al., 2011). However, the computational cost of least-squares migration (LSM) makes the application of this algorithm prohibitive for large-scale industrial 3D problems. Morton and Ober (1998) and Romero et al. (2000) proposed blended source migration where they blended several shotgathers into one supergather which is then migrated. This approach, although very effective in reducing the computational cost, suffers from crosstalk noise which severely degrades the quality of the migrated image. Later, Dai and Schuster (2009) and Schuster et al. (2011) extended the blended source migration technique to multisource least-squares migration and showed that the crosstalk noise can be mitigated by an iterative migration of supergathers.

In this paper, we propose using the seislet transform as a change of basis for reflectivity during multisource LSM. In addition, we also use a dip-constrained preconditioner which ensures that the image updates occur only along some pre-estimated dips or slopes. These dips or slopes are estimated from a standard migration image or from the gradient using a plane-wave destruction filter. Numerical tests on synthetic data show that this approach can efficiently suppress the crosstalk noise in multisource LSM and mitigate the aliasing artifacts caused by severely undersampled data.

THEORY

Under the single scattering Born approximation, the observed data, $\mathbf{d}$, can be written as

$$\mathbf{d} = \mathbf{L}\mathbf{m}. \tag{1}$$

Here $\mathbf{L}$ is the linearized Born modeling operator that predicts the data from the reflectivity image, $\mathbf{m}$. In conventional LSM, the reflectivity $\mathbf{m}$ is estimated by minimizing the misfit function, $\phi(\mathbf{m})$, given by (Nemeth et al., 1999)

$$\phi(\mathbf{m}) = \frac{1}{2}(\mathbf{L}\mathbf{m}-\mathbf{d})^T(\mathbf{L}\mathbf{m}-\mathbf{d}) + f(\mathbf{m}). \tag{2}$$

Here $f(\mathbf{m})$ is a regularization term that imposes constraints on the solution $\mathbf{m}$. If we express the reflectivity as a weighted sum of seislet basis functions, we have

$$\mathbf{m} = \mathbf{S}\hat{\mathbf{m}}. \tag{3}$$

Here $\mathbf{S}$ represents the inverse seislet transform and $\hat{\mathbf{m}}$ represents the seislet coefficients. After this transformation, equation 1 can be expressed as

$$\mathbf{d} = \mathbf{L}\mathbf{S}\hat{\mathbf{m}}, \tag{4}$$

and the objective function in equation 2 gets modified as

$$\phi(\hat{\mathbf{m}}) = \frac{1}{2}(\mathbf{L}\mathbf{S}\hat{\mathbf{m}}-\mathbf{d})^T(\mathbf{L}\mathbf{S}\hat{\mathbf{m}}-\mathbf{d}) + f(\hat{\mathbf{m}}). \tag{5}$$

If the prior model is of zero mean and known variance, then the regularization term $f(\hat{\mathbf{m}})$ can be expressed as

$$f(\hat{\mathbf{m}}) = \frac{1}{2}\hat{\mathbf{m}}^T C_{\hat{\mathbf{m}}}^{-1}\hat{\mathbf{m}}, \tag{6}$$

where $C_{\hat{\mathbf{m}}}$ represents the covariance of $\hat{\mathbf{m}}$. Thus, the objective function for estimating $\hat{\mathbf{m}}$ is given by

$$\phi(\hat{\mathbf{m}}) = \frac{1}{2}(\mathbf{L}\mathbf{S}\hat{\mathbf{m}}-\mathbf{d})^T(\mathbf{L}\mathbf{S}\hat{\mathbf{m}}-\mathbf{d}) + \frac{1}{2}\hat{\mathbf{m}}^T C_{\hat{\mathbf{m}}}^{-1}\hat{\mathbf{m}}. \tag{7}$$

DOI http://dx.doi.org/10.1190/segam2015-5869595.1

The gradient of equation 7 can be written as

$$\frac{\partial \phi(\hat{\mathbf{m}}_i)}{\partial \hat{\mathbf{m}}_i} = \mathbf{S}^T\mathbf{L}^T(\mathbf{LS}\hat{\mathbf{m}}_i - \mathbf{d}) + C_{\hat{\mathbf{m}}_i}^{-1}\hat{\mathbf{m}}_i, \tag{8}$$

and the corresponding normal equations are given by

$$\left(\mathbf{S}^T\mathbf{L}^T\mathbf{LS} + C_{\hat{\mathbf{m}}_i}^{-1}I\right)\hat{\mathbf{m}} = \mathbf{S}^T\mathbf{L}^T\mathbf{d}. \tag{9}$$

The matrices $\mathbf{S}^T$ and $\mathbf{S}$ can be implemented using the fast forward- and inverse-seislet transforms, respectively (Fomel and Liu, 2010). Hence, the choice of seislet transform as a suitable basis is appealing for a least-squares migration or full waveform inversion problem where it is not feasible to explicitly compute and store these matrices.

Multisource LSRTM using seislets

For multisource LSRTM, the relationship between the model and the data can be written as

$$\mathbf{NLm} = \mathbf{Nd}. \tag{10}$$

Here $\mathbf{N}$ represents the phase-encoding matrix associated with an ensemble of shot gathers. In a more compact notation, equation 10 can be written as

$$\mathbb{L}\mathbf{m} = \mathbb{D}, \tag{11}$$

where $\mathbb{L} = \mathbf{NL}$ and $\mathbb{D} = \mathbf{Nd}$. By expressing $\mathbf{m} = \mathbf{S}\hat{\mathbf{m}}$ we get

$$\mathbb{L}\mathbf{S}\hat{\mathbf{m}} = \mathbb{D}. \tag{12}$$

Adopting a similar approach as before, we can obtain the misfit function for multisource LSRTM using seislets as

$$\begin{aligned}\phi(\hat{\mathbf{m}}) &= \frac{1}{2}\left(\mathbb{L}\mathbf{S}\hat{\mathbf{m}} - \mathbb{D}\right)^T\left(\mathbb{L}\mathbf{S}\hat{\mathbf{m}} - \mathbb{D}\right) + \frac{1}{2}\hat{\mathbf{m}}^T C_{\hat{\mathbf{m}}}^{-1}\hat{\mathbf{m}}, \\ &= \frac{1}{2}\left(\mathbf{NLS}\hat{\mathbf{m}} - \mathbf{Nd}\right)^T\left(\mathbf{NLS}\hat{\mathbf{m}} - \mathbf{Nd}\right) + \frac{1}{2}\hat{\mathbf{m}}^T C_{\hat{\mathbf{m}}}^{-1}\hat{\mathbf{m}},\end{aligned} \tag{13}$$

and the gradient,

$$\begin{aligned}\frac{\partial \phi(\hat{\mathbf{m}}_i)}{\partial \hat{\mathbf{m}}_i} &= \mathbf{S}^T\mathbb{L}^T(\mathbb{L}\mathbf{S}\hat{\mathbf{m}}_i - \mathbb{D}) + C_{\hat{\mathbf{m}}_i}^{-1}\hat{\mathbf{m}}_i \\ &= \mathbf{S}^T\mathbf{L}^T\mathbf{N}^T(\mathbf{NLS}\hat{\mathbf{m}}_i - \mathbf{Nd}) + C_{\hat{\mathbf{m}}_i}^{-1}\hat{\mathbf{m}}_i.\end{aligned} \tag{14}$$

Preconditioning

For preconditioning, the approximate Hessian for equation 7 or equation 13 needs to be computed. The analytical expression for the Hessian in equation 7 is given by

$$\frac{\partial^2 \phi(\hat{\mathbf{m}}_i)}{\partial^2 \hat{\mathbf{m}}_i} = \mathbf{S}^T\mathbf{L}^T\mathbf{LS} + C_{\hat{\mathbf{m}}_i}^{-1}. \tag{15}$$

It is evident from equation 15 that computing the exact Hessian for the new misfit function in the transformed domain requires an explicit computation and matrix multiplication of the operators $\mathbf{L}$, $\mathbf{L}^T$, $\mathbf{S}$ and $\mathbf{S}^T$ which is prohibitive for realistic imaging problems. A useful approximation of the pseudo-inverse of the Hessian, also known as source and receiver side illumination compensation, has been shown to accelerate the convergence of LSM (Plessix and Mulder, 2004; Dai et al., 2012). Besides the source-side illumination preconditioner, we use two different kinds of preconditioners during the inversion.

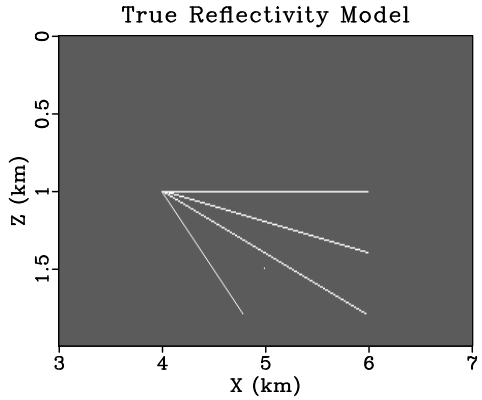

Figure 1: True reflectivity model used to generate the observed data.

- Thresholding the seislet coefficients to remove the unwanted artifacts in the image.
- Smoothing along the prominent dips in the image. The dips are estimated using plane-wave destruction filters (Claerbout, 1992; Fomel, 2002) and can be usually precomputed from the standard migration image or can be evaluated at every iteration from the gradient.

NUMERICAL RESULTS

We first demonstrate the effectiveness of using seislets for doing sparse LSM on an undersampled dataset. The observed data are generated using the reflectivity model shown in Figure 1 and with a homogeneous background velocity of 3500 m/s. There are only 10 shots generated which are evenly spaced at a distance of 1000 m on the surface and each shot is recorded by 50 receivers separated at an interval of 200 m.

Figures 2(a) and 2(b) compare the standard RTM and LSRTM images, respectively, for this sparse dataset. Unless otherwise mentioned, RTM usually refers to the image from the first least-squares iteration. It is evident from Figure 2(b) that LSRTM has improved the spatial resolution when compared to the RTM image. However, the aliasing artifacts are still not completely removed from the image. The RTM and LSRTM images using seislets are shown in Figures 2(c) and 2(d), respectively. It can be clearly seen that these images are free from the aliasing artifacts since the inversion using seislets promotes sparse image updates during the least-squares iterations.

We next show how seislets can be used during multisource LSRTM to mitigate the crosstalk noise. We simulate 256 shots using the true velocity model shown in Figure 3(a). Each shot is recorded with 512 receivers at a 20 m receiver interval with a total recording time of 10 s. We assume a fixed-spread acquisition geometry for both the sources and the receivers and blend all the 256 shotgathers into one supergather using the dynamic polarity and phase-encoding technique proposed by Schuster et al. (2011) and Dai et al. (2012). The velocity model shown in Figure 3(b) is used as the migration velocity model.

DOI http://dx.doi.org/10.1190/segam2015-5869595.1

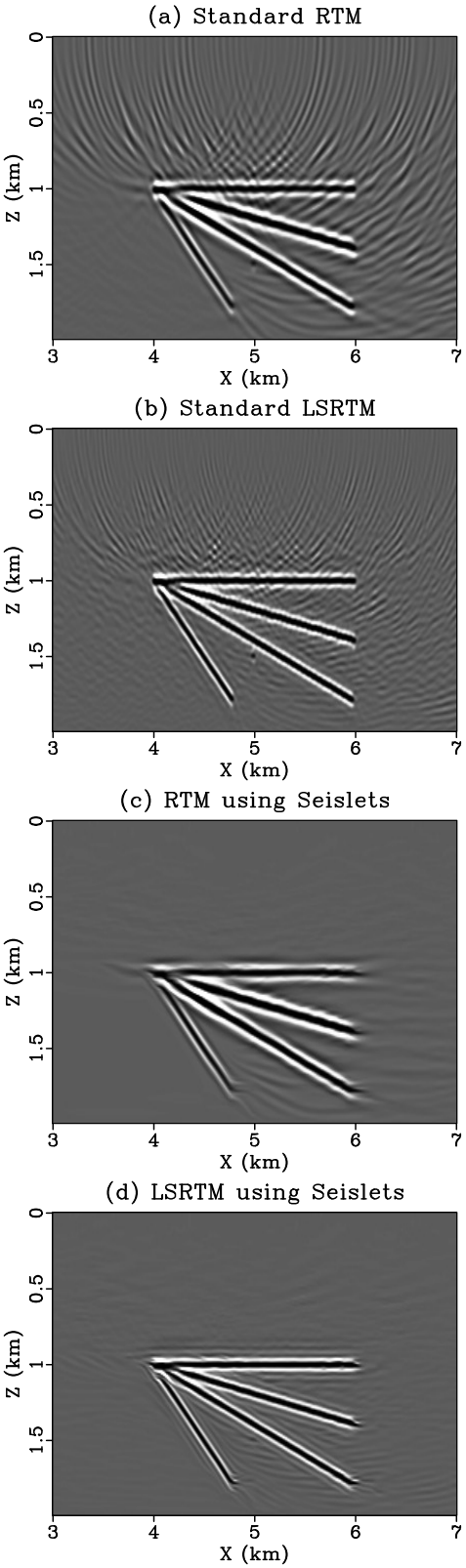

Figure 2: Images from (a) standard RTM, (b) standard LSRTM, (c) RTM using seislets, and (d) LSRTM using seislets. The LSRTM images are after 10 iterations.

Figure 4(a) shows the standard RTM image obtained by migrating each of the 256 shots individually. The local dips estimated from this RTM image are shown in Figure 4(b). Figures 5(a) and 5(b) show the standard multisource RTM and LSRTM images, respectively, using one supergather only. It can be seen that the crosstalk noise is dominant in the multisource RTM image. The SNR is relatively better in the multisource LSRTM image but the crosstalk noise is still prominent. The preconditioned multisource RTM and LSRTM images using seislets are shown in Figures 5(c) and 5(d), respectively. These images are free from the high-frequency crosstalk noise and the SNR is much better than the standard images.

CONCLUSIONS

A sparse least-squares migration technique is presented that uses the seislet transform as a change of basis for the reflectivity. Along with a dip-constrained preconditioner, this approach is shown to produce images with more meaningful structural updates during the least-squares iterations. Numerical tests on synthetic data for multisource LSRTM show that this technique can remove the crosstalk noise significantly from the image when using blended-source or multisource migration. Our numerical tests also show that the aliasing artifacts arising out of using undersampled data are also mitigated since the inversion promotes sparsity in the image during the least-squares iterations. The success of using seislets as basis functions during LSM significantly depends on the estimated dips. During inversion, care should be taken to ensure that the dip estimation is highly accurate.

ACKNOWLEDGEMENTS

We thank the sponsors of the Center for Subsurface Imaging and Modeling (CSIM) consortium for their support and KAUST Supercomputing Laboratory for providing the computational resources. The plots for this abstract have been prepared using the Madagascar open-source software package.

DOI http://dx.doi.org/10.1190/segam2015-5869595.1

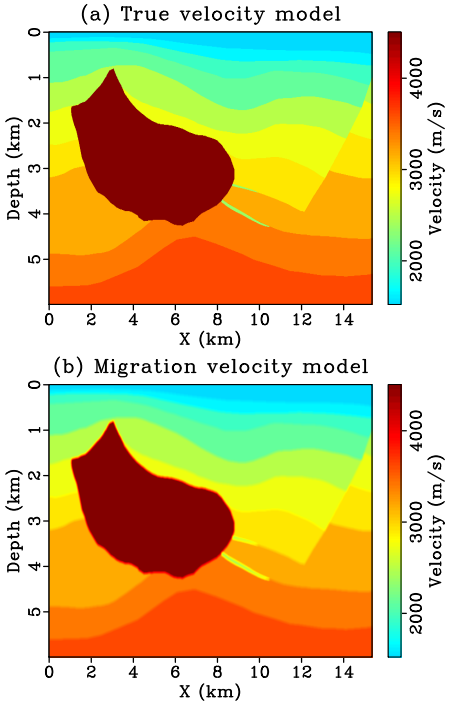

Figure 3: (a) True velocity model, and (b) migration velocity model.

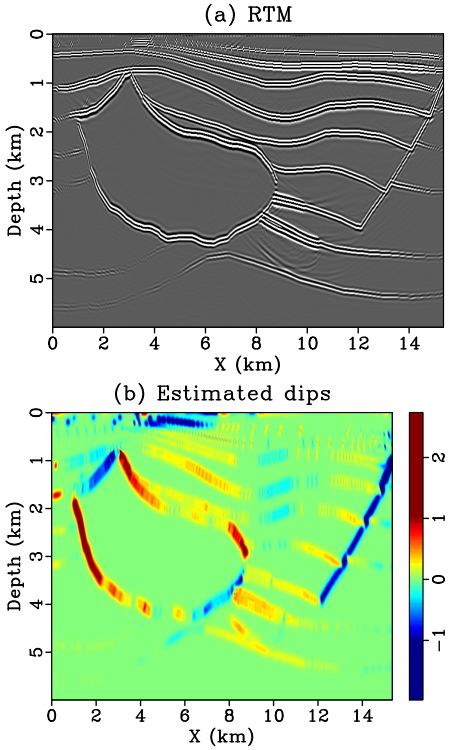

Figure 4: (a) Standard RTM image, and (b) estimated dips from the RTM image using plane-wave destruction filters.

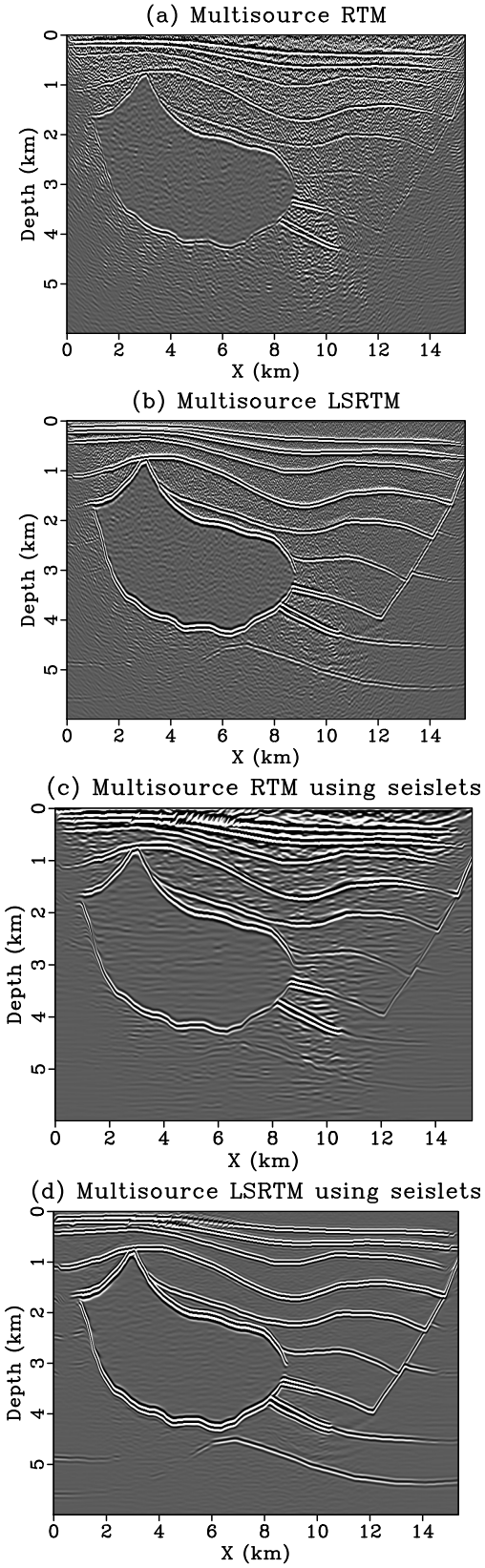

Figure 5: Images from (a) multisource RTM, (b) multisource LSRTM, (c) multisource RTM using seislets, and (d) multisource LSRTM using seislets. The LSRTM images are after 20 iterations.

DOI http://dx.doi.org/10.1190/segam2015-5869595.1

EDITED REFERENCES

Note: This reference list is a copyedited version of the reference list submitted by the author. Reference lists for the 2015 SEG Technical Program Expanded Abstracts have been copyedited so that references provided with the online metadata for each paper will achieve a high degree of linking to cited sources that appear on the Web.

REFERENCES

Abma, R., and N. Kabir, 2006, 3D interpolation of irregular data with a POCS algorithm: Geophysics, **71**, no. 6, E91–E97, http://dx.doi.org/10.1190/1.2356088.

Candès, E., L. Demanet, D. Donoho, and L. Ying, 2006a, Fast discrete curvelet transforms: Multiscale Modeling & Simulation, **5**, no. 3, 861–899, http://dx.doi.org/10.1137/05064182X.

Candès, E. J., J. K. Romberg, and T. Tao, 2006b, Stable signal recovery from incomplete and inaccurate measurements: Communications on Pure and Applied Mathematics, **59**, no. 8, 1207–1223, http://dx.doi.org/10.1002/cpa.20124.

Claerbout, J. F., 1992, Earth soundings analysis: Processing versus inversion: Blackwell Scientific Publications.

Dai, W., P. Fowler, and G. T. Schuster, 2012, Multisource least-squares reverse time migration: Geophysical Prospecting, **60**, no. 4, 681–695, http://dx.doi.org/10.1111/j.1365-2478.2012.01092.x.

Dai, W., and G. T. Schuster, 2009, Least-squares migration of simultaneous sources data with a deblurring filter: 79th Annual International Meeting, SEG, Expanded Abstracts, 2090–2994.

Dessing, F. J., 1997, A wavelet transform approach to seismic processing: Ph.D. dissertation, Delft University of Technology.

Duquet, B., K. J. Marfurt, and J. A. Dellinger, 2000, Kirchhoff modeling, inversion for reflectivity, and subsurface illumination: Geophysics, **65**, 1195–1209, http://dx.doi.org/10.1190/1.1444812.

Fomel, S., 2002, Applications of plane wave destruction filters: Geophysics, **67**, 1946–1960, http://dx.doi.org/10.1190/1.1527095.

Fomel, S., and Y. Liu, 2010, Seislet transform and seislet frame: Geophysics, **75**, no. 3, V25–V38, http://dx.doi.org/10.1190/1.3380591.

Foster, D. J., C. C. Mosher, and S. Hassanzadeh, 1994, Wavelet transform methods for geophysical applications: 64th Annual International Meeting, SEG, Expanded Abstracts, 1465–1468.

Herrmann, F. J., C. R. Brown, Y. A. Erlangga, and P. P. Moghaddam, 2009, Curvelet-based migration preconditioning and scaling: Geophysics, **74**, no. 4, A41–A46, http://dx.doi.org/10.1190/1.3124753.

Lailly, P., 1984, Migration methods: Partial but efficient solutions to the seismic inverse problem: Proceedings of the International Conference on Inverse Problems of Acoustic and Elastic Waves, 182–214.

Morton, S. A., and C. C. Ober, 1998, Faster shot record depth migrations using phase encoding: 68th Annual International Meeting, SEG, Expanded Abstracts, 1131–1134.

Nemeth, T., C. Wu, and G. T. Schuster, 1999, Least-squares migration of incomplete reflection data: Geophysics, **64**, 208–221, http://dx.doi.org/10.1190/1.1444517.

Plessix, R.-E., and W. A. Mulder, 2004, Frequency-domain finite-difference amplitude-preserving migration: Geophysical Journal International, **157**, no. 3, 975–987, http://dx.doi.org/10.1111/j.1365-246X.2004.02282.x.

Romero, L. A., D. C. Ghiglia, C. C. Ober, and S. A. Morton, 2000, Phase encoding of shot records in prestack migration: Geophysics, **65**, 426–436, http://dx.doi.org/10.1190/1.1444737.

Schuster, G. T., X. Wang, Y. Huang, W. Dai, and C. Boonyasiriwat, 2011, Theory of multisource crosstalk reduction by phase-encoded statics: Geophysical Journal International, **184**, no. 3, 1289–1303, http://dx.doi.org/10.1111/j.1365-246X.2010.04906.x.

Tang, Y., 2009, Target-oriented wave-equation least-squares migration/inversion with phase-encoded Hessian: Geophysics, **74**, no. 6, WCA95–WCA107, http://dx.doi.org/10.1190/1.3204768.

Wapenaar, K., R. Ghose, G. Toxopeus, and J. Fokkema, 2005, The wavelet transform as a tool for geophysical data integration: Integrated Computer-Aided Engineering, **12**, no. 1, 5–23.

Wong, M., S. Ronen, and B. Biondi, 2011, Least-squares reverse time migration/inversion for ocean bottom data: A case study: 81st Annual International Meeting, SEG, Expanded Abstracts, 2369–2373.